Hydrocarbon Deposition during Polyolefin Upcycling: Irreversible Adsorption and Surface Reactions of Polyethylene and Ethylene Oligomers on Silica Supports

Fawaz Motolani,[1] Rebekah J. Snellings,[2] Sogand Aghamohammadi,[1] Hee Jeung Oh,[1] Gina Noh,[1] Bert D. Chandler,[1,2] Bryan D. Vogt[1,]*

[1]Department of Chemical Engineering, The Pennsylvania State University, University Park, PA 16802 USA

[2]Department of Chemistry, The Pennsylvania State University, University Park, PA 16802 USA

*To whom correspondence should be addressed: bdv5051@psu.edu (B.D.V.)

ABSTRACT. Catalytic conversion of polyolefins to value-added products offers an alternative route to capture value from plastic waste. Here we initially examine reactions of a polyethylene model (hexatriacontane, $C_{36}H_{74}$) on a Pt/SiO_2 catalyst under typical hydrogenolysis and hydrocracking conditions, which leads to irreversibly adsorbed surface hydrocarbons after extraction with hot toluene. The IR spectra of these catalysts reveal only aliphatic C-H stretches. SiO_2 alone leads similar hydrocarbon adsorption on the surface where extended extraction fails to fully remove the adsorbed hydrocarbons from neat silica. The amount of hydrocarbon irreversibly adsorbed increases nearly tenfold when the reactant is changed from hexatriacontane to polyethylene (M_n = 4000 Da), but the adsorbed quantity is insensitive to reaction temperature (200-300 °C). These results demonstrate significant, non-extractable hydrocarbon deposition on catalyst support surfaces without dehydrogenation catalyst present at temperatures typical of catalytic deconstruction of polyolefin waste, which may limit catalyst turnover and impact the product distribution.

INTRODUCTION

Plastic waste represents a significant environmental challenge due to ever-growing plastics production[1-3] and inefficient end-of-life options that are dominated by landfilling and incineration.[4] Despite significant efforts in the recycling of plastic waste to reduce landfill burden and prevent microplastic release from landfill leachate,[5] plastic mismanagement, e.g., release into the environment, far surpasses the fraction of plastics that have been effectively recycled.[1] Plastic waste has been traded globally under the guise of recycling without clear regard for environmental impact,[6, 7] so a path to economic value from plastic waste is needed to improve resource management. Effective mechanical recycling methods are generally limited to just a few polymers such as poly(ethylene terephthalate) (PET) and high-density polyethylene (HDPE).[8, 9] Even for these, only about 1/3 - 1/2 of the HDPE that enters material recovery facilities (MRFs) can be effectively recovered for mechanical recycling; consequently, there is growing interest chemical recycling[10] or even upcycling[11] of plastic waste. These chemical routes convert plastic waste to liquid feedstocks or high-value products that offer the potential for circularity of carbon from the plastics in the economy.[12, 13]

Chemical recycling of plastics depends on the resin; step growth polymers, such as PET, are readily depolymerized to monomers, providing a direct route to circularity.[14] Other plastics, notably polyolefins, undergo side reactions before reaching temperatures sufficient for direct depolymerization.[10] As polyolefins comprise nearly 2/3 of all plastics produced,[15] there is an ongoing concerted effort to develop sustainable strategies for polyolefin chemical recycling or upcycling.[16, 17]

Pyrolysis offers a simple approach to the conversion of plastic waste to liquid oils,[18, 19] but is energy intensive and yields a complex mixture of liquids and char.[20] Catalytic approaches in the

chemical transformation of plastic waste offer opportunities to the reduce energy input[21] necessary for recycling[16] as well as the potential to better tune the output towards high-value products.[22, 23] These polyolefin chemical recycling approaches have generally focused on modifying the product distribution through catalyst design.[24, 25] For example, modifying a ruthenium surface with ethylene glycol enhanced the rate of C-C bond cleavage.[26] Despite these efforts, the low turnover rate due to transport limitations[27] and difficulty in product distribution control from heterogeneous plastic waste streams limit the commercial potential for catalytic cracking routes to enable circularity for the growing stream of polyolefin wastes. Recent work from Epps, Korley, and Vlachos has demonstrated the differences in the evolution in the molecular mass of polyolefin towards oligomers for catalytic and pyrolysis reactions to begin to better understand strategies to control the product distributions.[28]

Polyethylene adsorption onto catalyst surfaces has been suggested to be unfavorable due to the entropy of the polymer chains; this has also been implicated in destabilizing transition states.[29] However, polymers, notably polystyrene, have also been reported as being irreversibly adsorbed to silica surfaces.[30-32] Recently, Vlachos and coworkers reported the preferential adsorption of polyethylene over polypropylene on Ru-TiO_2 catalysts, as well as the segregation of higher molecular mass polyolefins on the catalyst surface.[33] These important insights were gleaned from molecular dynamics simulations and implied from the reaction products rather than via direct measurement. Additionally, precious metal catalysts used for polyolefin conversion (Pt, Ru) tend to be excellent dehydrogenation catalysts, and therefore promote the formation of coke and coke precursor species, which are well-known to foul the catalyst in gas phase dehydrogenation reactions.[34, 35]

Catalyst fouling occurs at lower temperatures with polyolefin reactants, and could arise from crosslinked polyolefins instead of coke-like aromatics.[34] Here we examine the adsorption and reaction of two alkanes (polyethylene and hexatriacontane, $\mathbf{C_{36}}$) on a model hydrogenolysis catalyst (Pt/silica) to understand the role of the metal and support on catalyst fouling. These experiments show evidence for the low-temperature reaction between alkanes and surface silanols, and thus provide new insights into the organic surface residuals on silica supported catalyst particles after chemical recycling. Both Fourier transform infrared spectroscopy (FTIR) and thermogravimetric analysis (TGA) indicate the accumulation of a substantial mass of organic material on the catalyst surface after reaction at 250 °C. Even when using $\mathbf{C_{36}}$ as the reactant feed, the reaction generated significant surface-bound residual organics that could not be removed with standard solvent product recovery methods.[21, 33, 36] FTIR spectra offered no evidence for the presence of aromatic coke-type species, and extended extraction in a good solvent for polyolefins failed to fully remove either polyethylene or $\mathbf{C_{36}}$. Control experiments using the silica support (i.e. no Pt present) showed similar or greater organic content as the Pt containing catalyst, suggesting reaction between the alkane and support hydroxyl groups anchors the alkane to the surface. These results illustrate surface reactions between polyethylene and catalyst supports can be significant and alter the catalyst surfaces regardless of the presence of precious metal catalysts. Including these interactions will likely be important for effective modeling of catalytic polyolefin upcycling processes.

EXPERIMENTAL SECTION

Materials: Silica (Davicat 1151, BET surface area: 274 $m^2\ g^{-1}$) was purchased from W.R. Grace and Company. Diamminedinitriplatinum(II) solution ($Pt(NH_3)_2(NO_3)_2$, 3.4 wt. % in dilute ammonium hydroxide), ammonium hydroxide (NH_4OH, 28.0-30.0% NH_3), dichloromethane

(DCM, ACS reagent ≥ 99.5%), p-xylene [$((CH_3)_2C_6H_4$, 99%], toluene [$C_6H_5CH_3$, ≥ 99.5%], decane [n-$C_{10}H_{22}$, ≥ 99%], polyethylene (PE, nominal M_w ≈ 4,000 Da, average M_n ≈ 1,700 Da, Product number: 427772, Batch number: MKCP9612) and n-paraffin mix of C_{18}, C_{20}, C_{22}, C_{24} (certified reference material, 2% (w/w) each component in octane) were purchased from Millipore Sigma. The polyethylene is likely low density based on the crystallinity (ca. 22 %) obtained from DSC measurements as shown in Figure S6. Acetone (ACS Reagent Grade, 99.5%) was purchased from Ricca Chemical. Hexatriacontane [**C_{36}**, n-$C_{36}H_{74}$, 97+%], dotriacontane [n-$C_{32}H_{66}$, 98%], octacosane [n-$C_{28}H_{58}$, 99%], and dodecane [n-$C_{12}H_{26}$, 99%] were obtained from ThermoFisher Scientific. Deionized (DI) water was obtained from a Milli-Q Direct-Q 3 UV Remote Water Purification System. Chemicals and materials were used as received, unless otherwise noted.

Catalyst Synthesis: Catalyst of Pt supported on SiO_2 (Pt/SiO_2, 1 wt% Pt) was synthesized by electrostatic adsorption based on literature procedures.[37] Briefly, $Pt(NH_3)_2(NO_3)_2$ (Sigma-Aldrich, 3.4 wt. % in dilute ammonium hydroxide) was deposited onto SiO_2 from 0.4 M NH_4OH solution. The slurry was stirred for 2 h to facilitate the adsorption of cationic Pt complexes. The solids were filtered and rinsed thrice with 100 mL of DI water. The metal loaded silica was heated in flowing air at 0.017 °C s^{-1} to 120 °C and held for 8 h. The dry Pt/SiO_2 was reduced to Pt clusters by heating under 5 mol% H_2 in Ar at 0.017 °C s^{-1} to 450 °C and holding for 3 h at 450 °C.

Hydrogenolysis / Adsorption: Hydrogenolysis of **C_{36}** was carried out in a sealed 2.4 mL autoclave reactor with a total headspace volume of 3.9 mL. Approximately 0.1 g of $C_{36}H_{74}$ and 0.05 g of either Pt/SiO_2 catalyst or neat SiO_2 were loaded into the reactor and heated to 100 °C to melt the **C_{36}**. The reactor was then purged with 4% H_2 in N_2 at 5 bar for 3 min, cyclically evacuated to 1 bar and re-pressurized to 5 bar four times to remove residual oxygen, and sealed. The sealed reactor containing 4% H_2 in N_2 was heated to 250 °C in a cylindrical furnace (National Element Inc.) using

a PID temperature controller (Auber-WS-1510DPMA). After the desired reaction time, the reactor vessel was quenched in an ice bath.

Three procedures were used to recover/remove organics from the catalyst particles. The reaction products were first soaked in 10 mL of dichloromethane (DCM) overnight at ambient temperature and filtered using Whatman filter paper to recover smaller hydrocarbon products (ca. C_6-C_{20}). The DCM fraction was analyzed with gas chromatography (GC). The inorganic solid + heavy residual hydrocarbon fraction was then dissolved in 20 mL of toluene at 100 °C and filtered (Whatman filter paper). This treatment is expected to extract the small polymers and waxes from the catalyst particles. A third extended extraction (~0.04 g silica) was performed using 2 mL of xylene at 120 °C for 1- 6 h. Xylene was selected for these exactions due to its high boiling point and good solvent characteristics for polyethylene and $\mathbf{C_{36}}$ at this temperature.

In a separate experiment, 0.1 g of polyethylene (PE) and 0.05 g of pure silica were loaded into the reactor and subjected to the same experimental conditions described above. After the desired heating time, the reactor vessel was quenched in an ice bath. The product was extracted for 1 h using 10 mL of xylene at 120 °C (± 3 °C); the liquid was then separated from the silica particles by vacuum filtration.

N_2 adsorption-desorption isotherms: Surface area measurements were performed on a Micromeritics 3Flex instrument at 77.3 K. Samples were degassed on a Micromeritics external VacPrep station by heating under active vacuum at 300°C overnight (2.7 °C min^{-1} ramp rate) then cooled to room temperature prior to data collection. The surface area was calculated using a multipoint Brunauer-Emmet-Teller (BET) method using the adsorption isotherms from $0.05 < P/P_0$

< 0.2. The silica surface area was determined to be 274 $m^2 \bullet g^{-1}$ from BET analysis as shown in Figure S15.

Transmission electron microscopy (TEM): Platinum particle sizes were determined by imaging with scanning/transmission electron microscopy (STEM) using a Talos F200C microscope at an accelerating voltage of 200 kV. To prepare each sample, a small quantity of catalyst was crushed in an agate mortar and pestle and dispersed in isopropanol via ultrasonification. A Cu TEM grid (Ted Pella, Inc.) was dipped into this suspension and allowed to dry before analysis. The average Pt nanoparticle diameter was determined using >300 particles using ImageJ software.

Gas chromatography: Reaction products recovered in DCM and toluene were analyzed with gas chromatography using an Agilent 7890A gas chromatograph outfitted with a 5m x 0.53mm x 0.17µm CP-SimDist UltiMetal column and flame ionization detector (GC-FID). A standard n-paraffin mixture (C_{18}, C_{20}, C_{22}, C_{24}) was used to calibrate the retention times for the column as shown in Figure S1. The response factor for quantifying the product peak areas was determined relative to dodecane for C_{10}, C_{18}, C_{28}, and C_{36} as shown in Figure S2.

For the analysis of reaction products, 200 µL of the extracted mixture was dissolved in 1.6 mL of either DCM or toluene (to match the extracted mixture) containing 10 µg of C_{12} per mL of DCM/toluene as the internal standard. For the mixture extracted with xylene, the solution was not further diluted due to the low concentration of hydrocarbons. The internal standard accounts for variations in injection volume, enabling quantitative mass balances on the system. These solutions were then analyzed with GC-FID. The product peaks were also confirmed with gas chromatography-mass spectrometry (GC-MS, Agilent 5975C mass spectrometer) with a 30 m x 250 µm x 0.1 µm VF-5ht column; mass spectra were compared to the NIST Mass Spectral Library

(Figure S3). The retention times and characteristic fragment ions were used to confirm the identity of each compound. Mass balances based on known loading and concentrations from GC analysis were used to determine hydrocarbon recovery.

FTIR: Transmission infrared spectra were recorded on a Bruker INVENIO R FTIR spectrometer. Each dried sample (13 mg) was pressed into a stainless steel wire gauze (100 x 100 mesh plain, 0.004" wire diameter) in a die using a pressure of 6 metric tons for 4 min. Each pellet was mounted into a controlled atmosphere transmission cell. All samples were heated *in situ* to 120 °C under flowing argon (40 mL min^{-1}) for ≈30 min to remove surface water. Spectra were recorded in absorbance mode at 120 °C at 1-min intervals until the spectral changes due to water desorption were no longer observed. The C-H stretching bands near 3000 cm^{-1} were integrated for each spectrum and converted to the hydrocarbon content using a calibration curve. The calibration curve relating the peak areas to percent weight hydrocarbon was developed by depositing known weights of several hydrocarbons ($C_{12}H_{26}$, $C_{18}H_{38}$, $C_{36}H_{74}$, and PE) dissolved in $CHCl_3$ onto neat SiO_2 pellets to provide a series of samples with different hydrocarbon:silica ratios that were pressed into pellets in the same manner as described above. Each calibration sample was dried in an oven at 80 °C to remove the solvent before collecting the FTIR spectra. A single linear correlation was found to describe the relationship between the peak area of the C-H stretching bands and the hydrocarbon concentration on SiO_2 for all hydrocarbons examined. This calibration curve (shown in Figure S7) that includes data from different hydrocarbons was used to determine the residual hydrocarbon on the catalyst or silica particles.

Thermogravimetric Analysis (TGA): Thermogravimetric analysis (TGA) of all samples was performed using a TA Discovery TGA 550 module. TGA curves were obtained under flowing N_2 (60 mL min^{-1}) with a heating rate of 20 °C min^{-1}. Sample masses between 4.0 - 6.0 mg were added

to a platinum pan and heated from 30 to 800 °C. Extracted SiO_2 and Pt/SiO_2 samples were held at 120 °C for 45 min to remove residual water from the particles during the ramp period. SiO_2 samples extracted with xylene were held at 140 °C for 45 min to remove residual solvent from the particles during the ramp period.

RESULTS AND DISCUSSION

Polyolefin waste consists of polymers with a wide diversity of molecular sizes and diversity of additives.[38, 39] Polymer molecular weight distributions and additives are commonly tuned to match specific applications.[40] This feedstock diversity presents a challenge to developing a fundamental mechanistic understanding of the cascade of processes that transform polyolefins into lower molecular mass hydrocarbons during chemical recycling.[28] To better understand the reactions, hexatriacontane ($C_{36}H_{74}$; **C_{36}**) was used as a molecularly well-defined oligomeric analog for polyethylene (Figure 1a). Typical polyolefin deconstruction catalysts consist of noble metal nanoparticles, particularly Pt and Ru, dispersed on high surface area oxide supports.[41] Figure 1b shows TEM data for the 1% Pt/SiO_2 catalyst used in this study; the Pt nanoparticles are well dispersed with an average diameter of 1.0 ± 0.2 nm (Figure 1c).

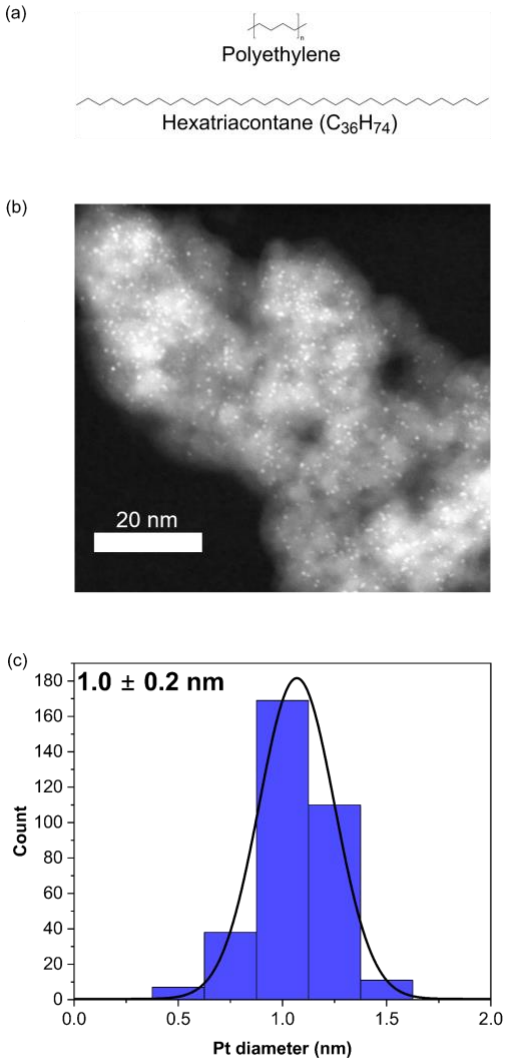

Figure 1. (a) Chemical structures of hexatriacontane and polyethylene. (b) Representative TEM image of synthesized 1% Pt/SiO_2 catalyst and (c) associated Pt particle size distribution (total counts: 335). The line shows a Gaussian fit to the TEM histogram.

Reactivity Measurements. Hexatriacontane is a high-purity saturated hydrocarbon with a melting point of 76 °C and is accessible to GC analysis (Figure 2a). As with larger polymers,

batch reactor studies require melting the reactant during the reaction. Unreacted **C_{36}** therefore remains mixed with the catalyst after reaction, presenting an analytical challenge. We addressed this by carefully measuring the catalyst and reactant masses before and immediately after the reaction. Masses determined immediately after reaction showed only minor mass losses, closing the carbon balance to within 1% (Table S1). Given the high precision and reproducibility of the carbon balance, minimal gas phase products (<1 %) are produced under these reaction conditions.

Consequently, the products of batch reactor studies can be quantified using GC (Figure 2a) by extracting product alkanes from the post-reaction mixture. Lighter hydrocarbons were extracted with dichloromethane (DCM). Hexatriacontane is only slightly soluble in DCM, but rapidly dissolves in hot (100 °C) toluene; lighter hydrocarbons remaining after DCM extraction will also dissolve in hot toluene. The reaction mixture was therefore subjected to a second extraction using hot toluene to remove the heavier hydrocarbons and any unreacted **C_{36}** from the catalyst. Figure 2b shows the chromatographs for the extractions using hot toluene. In all cases, only C_{36} reactants are observed, indicating that the DCM extraction effectively removed lighter products. The combination of these two extraction techniques, along with the closed global mass balance, allows us to use GC to garner information about reaction progress (see SI section on GC analysis for conversion and mass balance for more details).

Figure 2a shows the isolated products at all reaction times are almost exclusively octadecane ($C_{18}H_{38}$) and heptadecane ($C_{17}H_{36}$). The reaction conditions yield only modest amounts hydrogenolysis products (<1% total **C_{36}** conversion based on the concentrations of $C_{18}H_{38}$ and $C_{17}H_{36}$). The low yield is likely a result of the low H_2 concentration, low catalyst:reactant ratio, and lack of stirring during the reaction[42] as partitioning of H_2 into long alkane liquids is reasonable.[43] The reaction products indicate hydrogenolysis preferentially occurs at the center of

the alkyl chain. This is consistent with gas phase hydrogenolysis studies, which show entropy loses upon adsorption are minimized when relatively long segments near the end of the molecule are free (not adsorbed);[44, 45] this drives adsorption, dehydrogenation, and C-C bond cleavage near the center of the alkane chain. The two products appear in essentially equimolar ratios, suggesting an equivalent of methane is also produced. We note the conversions are low, making this hypothesized methane production difficult to directly observe; as evidence for this, the carbon balances are closed to within 1%.

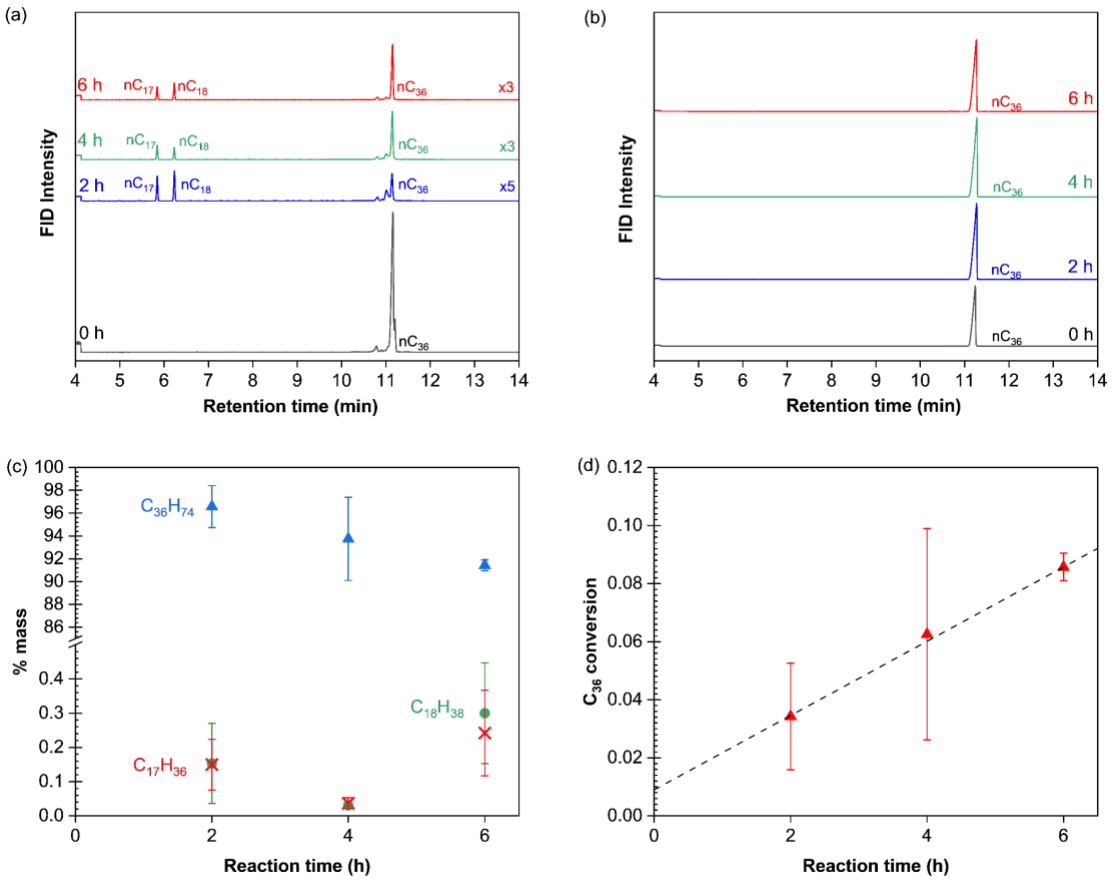

Figure 2. GC-FID analyses of reaction products recovered from the hydrogenolysis of hexatriacontane (n-$C_{36}H_{74}$) at different reaction times after initial extraction with (a) in DCM and subsequent extraction with (b) toluene, (c) mass (carbon) balance for $C_{36}H_{74}$ (▲), $C_{18}H_{38}$ (●), and

$C_{17}H_{36}$ (×) as a function of reaction time, (d) fractional conversion of $C_{36}H_{74}$ based on the $C_{36}H_{74}$ balance (▲). Reaction conditions: 250°C and 0.2 bar H_2 partial pressure.

Despite the low hydrogenolysis activity, Figure 2d shows a time dependent **C_{36}** conversion based on the **C_{36}** balance from GC. The conversion vs. time plot (Figure 2d) increases linearly, reaching approximately 8% conversion in 6 h. The plot also shows a non-zero intercept of ≈ 1% conversion, suggesting the onset of reactivity during the temperature ramp to 250 °C (≈ 17 min).

Quantification of Surface Hydrocarbons. The time dependent change in C_{36} mass, along with relatively consistent production of lower hydrocarbons, suggests the loss of **C_{36}** is associated with the generation of some sort of surface hydrocarbon species. The spent catalysts were therefore further characterized with TGA in N_2 (Figure 3a) and transmission IR spectroscopy (Figure 4). IR spectra confirm the presence of significant amounts of hydrocarbons on the catalyst after reaction and extraction (details below). The TGA data show a large decrease in mass near 300 °C for two of the specimens. Control experiments with neat **C_{36}** deposited onto silica (Figure S9) show mass loss at approximately the same temperature. This indicates the deposited hydrocarbons are (i) chemically similar to **C_{36}**, and (ii) thermally decompose / desorb in pathways similar to those for **C_{36}**. On average, Figure 3a indicates that there is a reduction in hydrocarbon on the surface at the longer time. Based on known dynamics for polymer chain adsorption,[46] the number of contacts tends to increase with time through flattening of molecules on the surface. This flattening of the molecule makes them more resistant to removal during extraction but reduces the available surface sites for adsorbed hydrocarbons with few contacts that are more easily removed. We hypothesize that a similar surface rearrangement mechanism is at play with the C_{36} that leads to a small

reduction in the amount of hydrocarbon left on the surface after extraction at longer reaction times. Figure 3b shows the residual hydrocarbon mass on the catalyst per surface area of SiO_2, which initially increases when the reaction time increases from 2 h to 4 h for both FTIR and TGA analyses. At longer times, the residual hydrocarbon mass decreases marginally from TGA analysis while the hydrocarbon content is not changed from FTIR analysis. The missing hydrocarbon mass calculated from the reaction mass balance measurements however increases monotonically with reaction time. If this missing mass is assumed to be C_{36} adsorbed on the catalysts, the difference with the direct analyses of the catalyst particles grows with reaction time but this analysis is prone to some error due to the small fraction of material that is unaccounted in the overall mass balance.

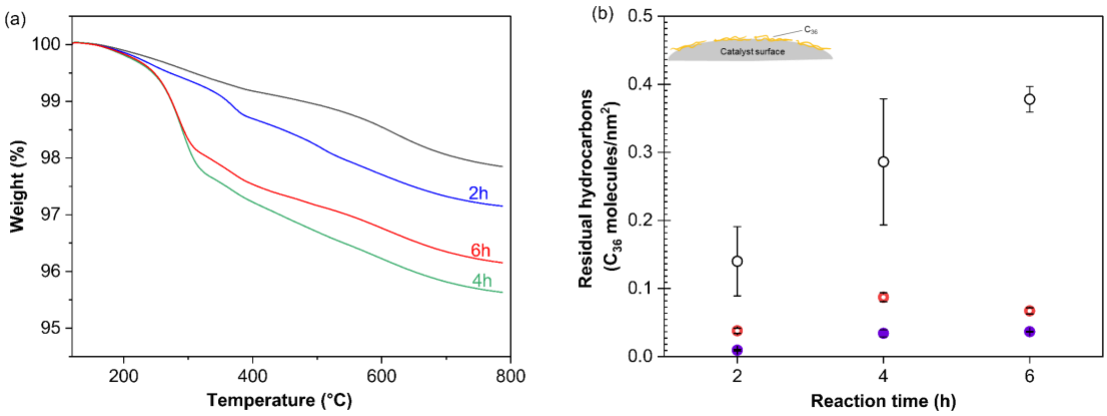

Figure 3. (a) TGA curves of neat Pt/SiO_2 (black) and the Pt/SiO_2 residue after 2 h (blue), 4 h (green), and 6 h (red) of reaction with the $C_{36}H_{74}$. (b) Hydrocarbon content per SiO_2 surface area on the Pt/SiO_2 as determined from (●) FTIR for the integrated C-H peak areas and (⭘) TGA on the basis that the residual hydrocarbons are $C_{36}H_{74}$. From mass balance calculations, the missing hydrocarbon including mass loss during recovery from reaction vessel and mass on the catalyst surface (○) was assumed to be $C_{36}H_{74}$ and normalized by the SiO_2 surface area for direct comparison to analyses of the residual catalysts.

FTIR spectroscopy of the post-reaction catalyst particles (Figure 4) also provides insights into the surface species formed during the reaction. The spectrum of the as-synthesized Pt/SiO_2 catalyst (Figure 4a) showed no appreciable hydrocarbons on the surface. After the reaction, there are clear peaks between 3000 and 2800 cm^{-1} corresponding to aliphatic C-H stretches (the nature of the surface hydrocarbons is discussed below). The insets in Figure 4b – d highlight wavenumber band (3000 - 3300 cm^{-1}) typically associated with aromatic C-H stretches. The absence of peaks in this range indicates that no aromatic compounds were produced. Transmission IR can be a quantitative spectroscopic technique with proper normalization, so the Si-O-Si bands near 1650 cm^{-1} can serve as an internal standard to normalize the surface C-H stretches. This analysis shows the C-H stretching area increases significantly on increasing the reaction time from 2 h to 4 h (Table S2). The IR data was also quantified using the calibration curve from linear alkanes - silica mixtures (Figure S7) for direct comparison of the quantitative TGA, FTIR, and mass balance data, shown in Figure 3b.

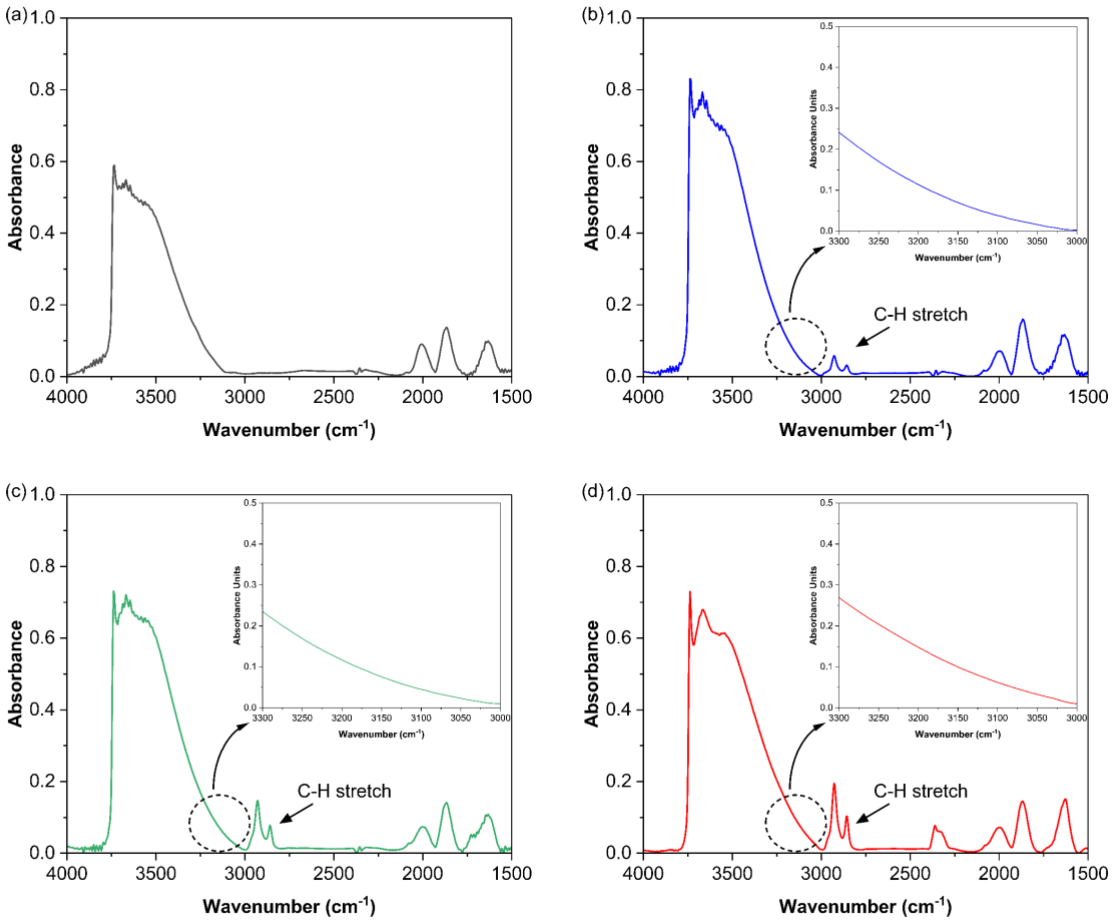

Figure 4. FTIR spectra of (a) original as-synthesized Pt/SiO_2 catalyst and the residual washed Pt/SiO_2 catalyst after (b) 2 h, (c) 4 h, and (d) 6 h of reaction at 250 °C. The insets highlight the wavenumber band (3000-3300 cm^{-1}) region corresponding to aromatic C-H stretches.

Nature of Surface Hydrocarbons. Hydrocarbon deposition during reaction is commonly attributed to coking, which is generally considered as surface aromatization leading to pre-graphitic structures.[34, 35] For these catalysts, however, the observed C-H stretching frequencies correspond to aliphatic, not aromatic hydrocarbons. The insets in Figure 4 highlight the aromatic C-H stretching region; the IR spectra show no evidence for the presence of aromatics on the

surface. Several additional observations make it difficult to characterize the deposited hydrocarbons as coke. First, the post-reaction C-H stretches are virtually indistinguishable from the reactant C-H vibrations, suggesting the deposited species are chemically similar to the parent **C$_{36}$** molecule. Second, the decomposition temperature for **C$_{36}$** and the adsorbed hydrocarbons in the TGA experiments are essentially the same, indicating likely similar structures. The decomposition temperature is also considerably lower than temperatures typically used to remove coke and coke precursors, even under O_2 atmospheres.[47, 48] Third, coking is typically associated with poisoning of metal surfaces and a loss of reactivity. In this case, **C$_{36}$** conversion increases linearly over 6 h of reaction time; this behavior is indicative that the minimal coking/hydrocarbon adsorption on the catalyst does not appreciably impact the reaction kinetics. The reaction temperature (250 °C) is lower than what is typically reported for dehydrogenation with precious metals like Pd and Pt.[49, 50]

Based on these observations, it is difficult to reasonably describe the deposited hydrocarbons as coke or coke precursors, and the surface hydrocarbons from **C$_{36}$** reactions appear to be deposited via a different mechanism than coke formation processes. Condensation and oligomerization reactions are more commonly observed than aromatization processes at low temperatures (< 200 °C),[34] so the deep dehydrogenation pathways that lead to coke precursors may not be accessible for the Pt/SiO_2 catalyst at 250 °C. The presence of liquid hydrocarbons on the catalyst surface may also impede coke formation, particularly if coke precursors are partially solubilized or solvated by the surface and liquid hydrocarbons. This is an added complexity to polyolefin hydrogenolysis that is not present in traditional gas phase reactions.

Reactivity of Silica Surfaces. Our results raise several questions regarding the nature of the hydrocarbon residue on the surfaces. The deposited hydrocarbon masses, which approach 10 wt.

% (relative to the catalyst from Figure 3b) for the longest reaction times, are far too massive to only be associated with the Pt nanoparticles. We therefore performed a series of control experiments examining the reactivity of **C$_{36}$** with the silica support. As the coking is typically driven by catalytic reactions,[51] the **C$_{36}$** was heated with the silica support material at 250 °C and H_2 to mimic hydrogenolysis conditions; samples were then extracted with hot toluene as described previously for the Pt/SiO_2 catalyst. The FTIR spectra (Figure 5a) shows significant residual aliphatic hydrocarbons with no identifiable aromatic peaks. These spectra are similar to those obtained with the Pt catalyst (Figure 4). TGA studies of the extracted silicas confirmed the hydrocarbon content; Figure 5b shows the FTIR and TGA data from the silica reactions are well correlated. FTIR spectra of the silica particles collected after the TGA measurement also show no signs of aromatic hydrocarbons (Figure S10), indicating that the surface hydrocarbons do not convert to graphitic structures in N_2 at elevated temperatures.

The silica support showed the highest hydrocarbon content (≈ 7 wt.%) at the shortest reaction time, suggesting the deposited hydrocarbons are not stable under the reductive reaction conditions. Assuming a surface footprint of ~0.5 nm^2 per **C$_{36}$**, this corresponds to a roughly 15-20% surface coverage of the silica, and provides a reasonable explanation for the low activity of the Pt catalyst. Hydrocarbon deposition onto silica is considerably faster than hydrogenolysis under these conditions, so it is likely the Pt particles are at least partially blocked by the residues before hydrogenolysis can take place. It is intriguing that the presence of Pt appears to slow the hydrocarbon deposition.

More importantly, these experiments clearly identify a reaction pathway between hydrocarbons and oxide supports that is not generally considered in polymer upcycling studies. Note our studies are intentionally performed under low H_2 pressure to promote coke formation, yet none is

observed. Rather, irreversible (see below) hydrocarbon deposition onto the support occurs at low temperatures; given silica cannot activate H_2, it is unlikely the reaction is at all impacted by the hydrogen pressure. The vast majority of polymer upcycling studies utilize batch reactors loaded and pressurized at ambient temperature, then heated to the high temperature and pressure operating conditions of the catalyst. During the temperature ramp, the catalysts likely pass through an operating regime similar to the conditions used in our experiments before reaching higher operating temperatures. If polyethylene can adsorb irreversibly to a silica support, and this interaction takes hold before the hydrogenolysis activity on the metal can start, this support-plastic interaction should be considered in interpreting catalytic activity and modeling catalytic upcycling reactions.

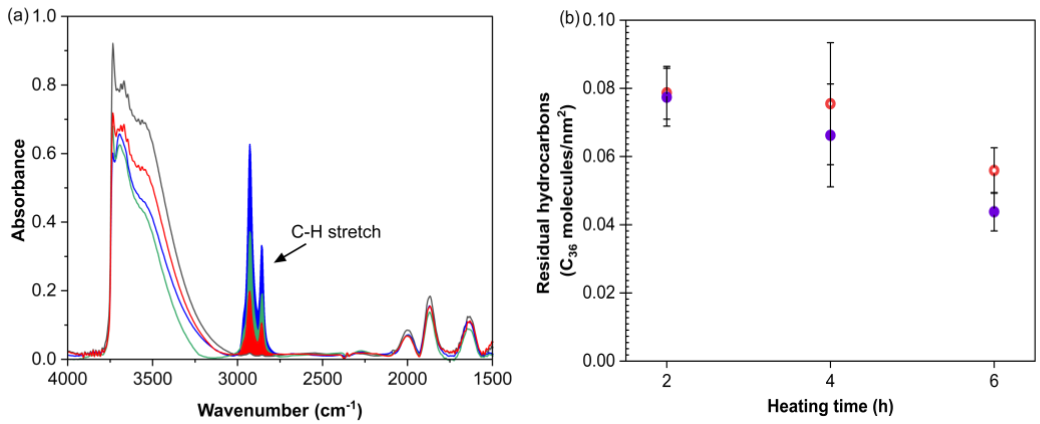

Figure 5. (a) FTIR spectra of unreacted SiO_2 (black) and SiO_2 residue after heating with $C_{36}H_{74}$ for 2h (blue), 4h (green), and 6 h (red) at 250 °C. (b) Mass of residual hydrocarbons on neat SiO_2 particles as a function of heating time at 250 °C as determined from (●) FTIR for the integrated C-H peak areas and (⭘) TGA

We considered three likely possibilities for the hydrocarbon deposition during **C_{36}** reactions: (i) alkane crosslinking at elevated temperatures to yield larger polyolefins; (ii) exceptionally strong

non-dissociative adsorption of the alkane chains at elevated temperatures; and (iii) surface reaction with surface silanols or Si-O-Si bonds. To clarify our terminology, we specifically refer to non-dissociative adsorption as an adsorption event where no C-H bonds are broken to distinguish this process from a surface reaction, which likely breaks at least one C-H bond and one surface bond.

In some cases, polymer adsorption can be effectively irreversible (i.e. non-dissociative irreversible adsorption),[30, 31] providing a potential explanation for the aliphatic hydrocarbon deposition we observe. For example, polystyrene adsorption on silicon wafers shows an initial increase in the polymer content during annealing;[52] this study found the adsorption rate is determined by polymer mobility.[53] Large polymers have multiple polymer-support interactions and have a propensity for developing inter-chain entanglements. However, **C$_{36}$** is very small relative to a polymer, so the potential number of segmental interactions per molecule is limited and, based on the entanglement molecular mass for polyethylene, there is no potential for entanglements with **C$_{36}$**.[54]

The irreversible adsorption of polymers is generally elucidated by extensive, prolonged extraction processes; the time scale for extraction of polymer tends to be much longer than typical reports for solids extraction during polymer upcycling.[21, 33, 36] A control experiment, in which **C$_{36}$** was melted on SiO_2 at 80 °C for 5 min and subsequently extracted with toluene at 100 °C, confirmed the complete removal of **C$_{36}$** from the SiO_2 surface, as evidenced by IR analysis as shown in Figure S11. These results demonstrate that the irreversible hydrocarbon deposition requires exposure to high temperatures.

We performed a more aggressive extraction to remove any strongly (physically) adsorbed **C$_{36}$** or longer chains from radical-driven branching reactions.[52, 55-57] The post-reaction silica particles (no Pt) were further rinsed with hot (120 °C) xylene, which readily dissolves

polyethylene.[52, 55-58] Figures 6a and S12 show TGA curves for these extracted silica particles. Figure 6c presents a parity plot for the two techniques (TGA and FTIR), showing the residual hydrocarbon mass on silica (no Pt) is consistent by the two independent measures.

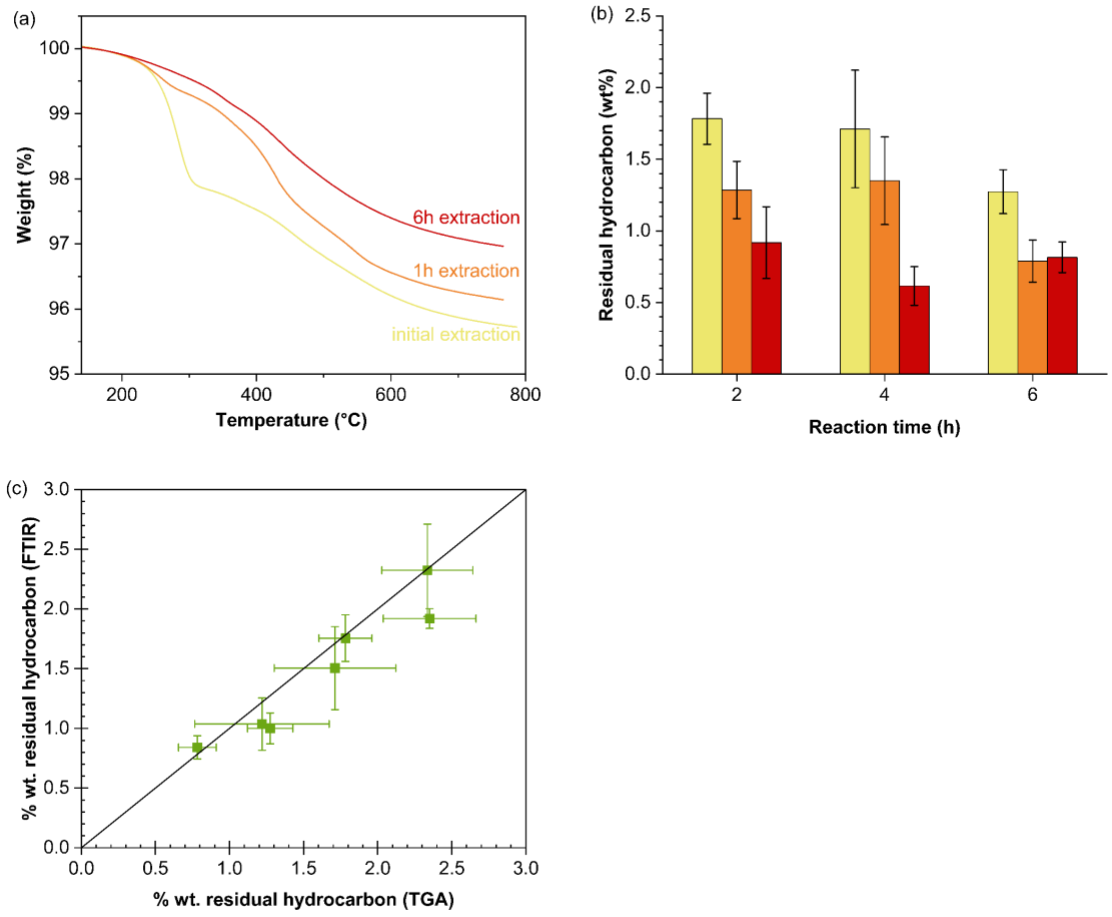

Figure 6. (a) TGA traces for SiO_2 particles after heating with **C_{36}** for 4 h at 250 °C (b) Adsorbed hydrocarbon content on the SiO_2 particles after initial extraction with DCM and toluene (yellow) and subsequent extraction in xylene at 120 °C for 1 h (orange) and 6 h (red). The adsorbed hydrocarbon content is dependent on heating time at 250 °C initially and was determined by TGA (c) Parity plot for residual hydrocarbon adsorbed on SiO_2 particles as determined by TGA and

FTIR measurements. The black line represents the expected 1:1 relationship (y = x), indicating agreement between the two methods.

Three observations from these data are of note. First, the hot xylene extraction removed additional hydrocarbons from the surface. Second, additional time under hot xylene generally removed additional hydrocarbons except in the case for 6 h of reaction. Third, regardless of the **C_{36}** reaction time, after 6 h of extraction in hot xylene, a substantial and relatively consistent amount of hydrocarbons (≈ 0.7 wt.%) remained on the surface. This corresponds to a surface coverage of approximately 0.031 molecules of **C_{36}** per nm^2, or a silica surface coverage of approximately 2%.

These data lend themselves to several conclusions. First, the hydrocarbons remaining after 6 h of hot xylene extraction can be characterized as irreversibly adsorbed species. Unlike large polymers,[30, 31] we can find no process by which a relatively small **C_{36}** molecule can adsorb irreversibly without surface reaction to anchor the hydrocarbons. This is most likely due to a surface reaction with silica silanols, which need only generate one Si-O-C bond to effectively immobilize the hydrocarbon. This is consistent with the IR observations, indicating the majority of the C-H stretches are unaffected by deposition.

Alternatively, radical branching of polyethylene would be expected at 250 °C; if radicals are stabilized on the silica and these radicals promote multiple branching of adsorbed species, a crosslinked islands of polymers/hydrocarbons on the silica could be generated. These larger MW hydrocarbons/polymers would look more like polyethylene in their thermal characteristics. The

TGA data, which shows increases in the temperature required to remove the remaining hydrocarbons after extraction (Figure 6a) is consistent with this conclusion.

Second, hot xylene successfully removed some of the deposited hydrocarbons. While it is possible the DCM and toluene extraction processes were too short to effectively remove physically adsorbed $\mathbf{C_{36}}$ from the surface, this seems unlikely given our repeated control experiments. This includes attempts at direct adsorption of $\mathbf{C_{36}}$ from dodecane solution. Multiple attempts showed no direct adsorption, confirming $\mathbf{C_{36}}$-silica interactions are relatively weak. What seems more likely is either larger hydrocarbons are present on the surface, or the xylene treatment removes some anchored hydrocarbons, perhaps through hydrolysis reactions with trace water in the solvent. The TGA data in Figure 6 is consistent with both possibilities. There is some correlation in the temperature for the mass loss for the silica after the toluene extraction and the amount of hydrocarbon extracted by the hot xylene as shown in Figure S13. This is indicative of different species on the silica where their thermal stability is correlated with potential for extraction in hot xylene. Examination of the xylene extract by GC-FID indicated that $\mathbf{C_{36}}$ were removed from the silica (Figure S14).

We favor these explanations, or perhaps a combination of the two, because they can largely be attributed to the generation of a few radical species at high temperatures. This is also appealing because it provides at least a potential mechanism for the metal to slow hydrocarbon deposition onto the surface, simply by scavenging reactive radicals. Additionally, while it is reasonable to consider polymer adsorption to be effectively irreversible when hundreds of polymer segment-support interactions occur simultaneously, we know of no comparable mechanism that would allow non-activated adsorption of $\mathbf{C_{36}}$ induce similar strong adsorption. However, we cannot rule

out the possibility that there is a strongly adsorbed (non-activated) **C$_{36}$** species present on the surface.

With the general framework developed for **C$_{36}$**, we examined hydrocarbon deposition on silica from a low molecular mass (4 kDa) polyethylene. Our goal was to better understand the differences in the adsorption between long alkanes and polymers on catalyst support surfaces and extend our insights to conditions relevant to polyolefins upcycling. Figure 7 shows the irreversibly adsorbed or anchored hydrocarbon surface coverage for **C$_{36}$** and ≈ 4 kDa polyethylene, i.e. the surface normalized mass of hydrocarbon remaining after hot xylene extraction for 1 h. The reaction (deposition) time was held constant at 2 h while the reaction (deposition) temperature was varied from 200 to 300 °C.

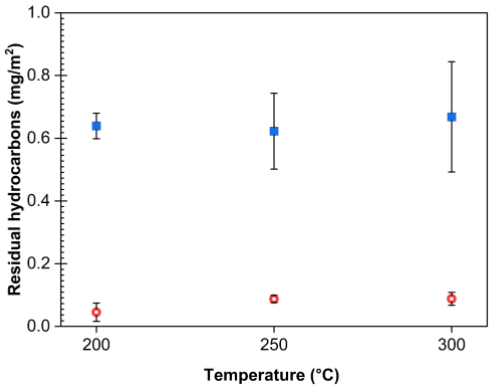

Figure 7. Role of temperature on the amount of residual hydrocarbon on SiO_2 for (⭕) $C_{36}H_{74}$ and (■) polyethylene after extraction for 1 h with xylene at 120 °C.

In both cases, the hydrocarbon deposition is essentially insensitive to the reaction temperature, suggesting the reaction is complete and the surface is fully covered at 200 °C after 2 h. This is consistent with the temperature window for condensation and chain transfer reactions, which are more common than coke formation reactions at low temperatures.[34] Relative to the **C$_{36}$**, the polyethylene deposits an order of magnitude more material on the silica surface. This increased

apparent polymer adsorption on surfaces is consistent with theory of polymer adsorption for molecular mass dependencies.[59, 60] Perhaps more importantly, the order of magnitude increase is consistent with the order of magnitude difference in molecular weights (4000 Da vs 590 Da). Thus, approximately the same number of hydrocarbon chains are anchored in the reaction. This suggests a comparable number of radicals are generated, which is reasonable considering both reactions used equivalent masses of chemically similar C-H bonds. These data illustrate the often-overlooked importance of the catalyst support on the products obtained from catalytic deconstruction of polyolefin waste. Irreversible adsorption can clearly occur despite the lack of strong specific interactions, and radical chemistry may become more important at elevated temperatures. It should be noted that the exact details of these surface reactions and the polymer adsorption may be dependent on the exact nature of the support. Future work will examine how other supports, such as alumina and acidic zeolites, impact the residual polyethylene on the surface after heating.

CONCLUSIONS

This study identifies an under-reported low-temperature reaction pathway between silica support surfaces and long-chain alkanes or polymers; this pathway is generally not considered in modeling polymer upcycling reactions, yet occurs under conditions most catalytic studies pass through. We found significant quantities of residual hydrocarbons on silica supports after performing catalytic polyolefin deconstruction reactions under conditions relevant to the upcycling of plastic waste. Using polyethylene and a model oligomer reactant, independent TGA and FTIR measurements, as well as careful mass balance determinations, confirmed the presence of surface hydrocarbons after heating with $\mathbf{C_{36}}$ to 250 °C under H_2. The FTIR spectra of silica and Pt-silica particles after extraction with DCM and hot toluene exhibited clear C-H stretch bands. There were no qualitative

differences in the residual hydrocarbons on silicas with and without Pt, indicating hydrocarbon deposition occurred on the support. This result is inconsistent with expected coking mechanisms associated with hydrogenolysis, as these mechanisms rely on dehydrogenation pathways on the precious metal catalyst. Both TGA and IR confirmed typical extraction practices used for recovery of non-polymeric products in catalytic deconstruction of polyolefins[21, 33, 36] were unable to extract all of the post-reaction hydrocarbons from the surface. Even after 6 h of extraction in excess xylene at 120 °C, approximately 1 wt% hydrocarbon remained on the silica surface. This demonstrates that some $\mathbf{C_{36}}$ is effectively irreversibly adsorbed to the silica surface, despite no apparent change in the chemistry probed by IR spectroscopy and TGA. We propose two potential mechanisms for the unextractable hydrocarbons, both of which may be involved: (i) radical driven surface attachment of $\mathbf{C_{36}}$ to surface silanols and (ii) radical stabilization on the silica generates multiple branching reactions on the adsorbed $\mathbf{C_{36}}$ to effectively crosslink the hydrocarbon to the silica.

Similarly, reactions using a low molecular mass polyethylene ($M_w \approx 4$ kDa) also generated hydrocarbons on the silica that could not be removed via extraction. Under the same conditions (250 °C, 2 h), the polyethylene results in an order of magnitude higher amount of residual hydrocarbon on the silica; this value is consistent with the order of magnitude higher molecular weight of polyethylene. The amount of polyethylene or $\mathbf{C_{36}}$ on the silica was effectively independent of temperature over the range examined, 200 °C – 300 °C, suggesting the surface reaction occurs at moderate temperatures. In aggregate, these results demonstrate the strongly bound hydrocarbons on catalytic supports generated during chemical recycling of polyolefin waste may not necessarily be attributable to reactions associated with the catalyst. Rather, the polymers and related species can interact with the silica support surface to produce effectively irreversibly

adsorbed or anchored hydrocarbons. We hypothesize radical reactions at the interfaces may be responsible for initiating the anchoring reactions. Consequently, support-plastic interactions at elevated temperatures should be considered in the development of catalyst systems for catalytic plastic recycling/upcycling as these tethered polymers may be detrimental to catalyst performance. Additional work is needed to determine the generalizability of these findings across the variety of support chemistries common in plastic upcycling.

ASSOCIATED CONTENT

Supporting Information. Quantification of pre- and post-reaction masses for **C_{36}** reaction over Pt/SiO_2 catalyst, silica, and PE over silica, GC retention time calibration and relative response factors, Mass spectra of reaction products from GC-MS, TGA traces for hexatriacontane and polyethylene, DSC curve for polyethylene, Calibration curve for the concentration of alkanes on silica, Full FTIR spectra of as-synthesized Pt/SiO_2 catalyst and residual washed Pt/SiO_2 catalyst, C-H stretch integrated areas on Pt/SiO_2 residue from FTIR, Surface footprint of C_{36} calculation, Residual hydrocarbon content calculation, TGA curves of neat silica and silica residues, FTIR of silica after TGA measurements, FTIR spectra of silica particles used in the control experiment, TGA curves of extracted (in xylene at 120 °C for 1h and 6h) silica particles, Parity plot for mass loss in TGA between 260 and 310 °C and **C_{36}** extracted in xylene at 120 °C, GC-FID trace of xylene extract from silica particles, N_2 adsorption isotherm of silica particles. (PDF)

AUTHOR INFORMATION

Corresponding Author

* bdv5051@psu.edu (B.D.V.)

Author Contributions

The manuscript was written through contributions of all authors. All authors have given approval to the final version of the manuscript.

ACKNOWLEDGMENT

This work was partially supported by the National Science Foundation under grant CBET - 2229168. The authors acknowledge the Penn State Materials Characterization Lab for use of the Talos F200C STEM and Audrey Battiste for assisting with TEM data collection and analysis. The assistance of Brendan Troesch with BET measurements is acknowledged.

REFERENCES

(1) Geyer, R.; Jambeck, J. R.; Law, K. L. Production, use, and fate of all plastics ever made. **2017**, *3* (7), e1700782. DOI: doi:10.1126/sciadv.1700782.

(2) Walker, T. R.; Fequet, L. Current trends of unsustainable plastic production and micro(nano) plastic pollution. *TrAC, Trends Anal. Chem.* **2023**, *160,* 116984. DOI: 10.1016/j.trac.2023.116984.

(3) Tiwari, R.; Azad, N.; Dutta, D.; Yadav, B. R.; Kumar, S. A critical review and future perspective of plastic waste recycling. *Sci. Total Environ.* **2023**, *881*, 163433. DOI: 10.1016/j.scitotenv.2023.163433.

(4) Kibria, M. G.; Masuk, N. I.; Safayet, R.; Nguyen, H. Q.; Mourshed, M. Plastic Waste: Challenges and Opportunities to Mitigate Pollution and Effective Management. *Int. J. Environ. Res.* **2023**, *17* (1), 20. DOI: 10.1007/s41742-023-00507-z.

(5) Kabir, M. S.; Wang, H.; Luster-Teasley, S.; Zhang, L. F.; Zhao, R. Z. Microplastics in landfill leachate: Sources, detection, occurrence, and removal. *Environ. Sci. Ecotechnology* **2023**, *16,* 100256. DOI: 10.1016/j.ese.2023.100256.

(6) Liang, Y. Y.; Tan, Q. Y.; Song, Q. B.; Li, J. H. An analysis of the plastic waste trade and management in Asia. *Waste Manage.* **2021**, *119*, 242-253. DOI: 10.1016/j.wasman.2020.09.049.

(7) Li, K.; Ward, H.; Lin, H. X.; Tukker, A. Traded Plastic, Traded Impacts? Designing Counterfactual Scenarios to Assess Environmental Impacts of Global Plastic Waste Trade. *Environ. Sci. Technol.* **2024**, *58* (20), 8631-8642. DOI: 10.1021/acs.est.4c02149.

(8) Oblak, P.; Gonzalez-Gutierrez, J.; Zupancic, B.; Aulova, A.; Emri, I. Mechanical Properties of Extensively Recycled High Density Polyethylene. In *Annual Conference and Exposition of*

Society-for-Experimental-Mechanics on Experimental and Applied Mechanics, Costa Mesa, CA, Jun 08-11, 2015; Springer: NEW YORK, 2016; pp 203-208. DOI: 10.1007/978-3-319-21762-8_24.

(9) Stegmann, P.; Gerritse, T.; Shen, L.; Londo, M.; Puente, A.; Junginger, M. The global warming potential and the material utility of PET and bio-based PEF bottles over multiple recycling trips. *J. Cleaner Prod.* **2023**, *395,* 136426. DOI: 10.1016/j.jclepro.2023.136426.

(10) Coates, G. W.; Getzler, Y. Chemical recycling to monomer for an ideal, circular polymer economy. *Nat. Rev. Mater.* **2020**, *5* (7), 501-516. DOI: 10.1038/s41578-020-0190-4.

(11) Korley, L. T. J.; Epps, T. H.; Helms, B. A.; Ryan, A. J. Toward polymer upcycling - adding value and tackling circularity. *Science* **2021**, *373* (6550), 66-69.

(12) Worch, J. C.; Dove, A. P. 100th Anniversary of Macromolecular Science Viewpoint: Toward Catalytic Chemical Recycling of Waste (and Future) Plastics. *ACS Macro Lett.* **2020**, *9* (11), 1494-1506. DOI: 10.1021/acsmacrolett.0c00582.

(13) Chen, H.; Wan, K.; Zhang, Y. Y.; Wang, Y. Q. Waste to Wealth: Chemical Recycling and Chemical Upcycling of Waste Plastics for a Great Future. *Chemsuschem* **2021**, *14* (19), 4123-4136. DOI: 10.1002/cssc.202100652.

(14) Geyer, B.; Lorenz, G.; Kandelbauer, A. Recycling of poly(ethylene terephthalate) - A review focusing on chemical methods. *EXPRESS Polym. Lett.* **2016**, *10* (7), 559-586. DOI: 10.3144/expresspolymlett.2016.53.

(15) Vogt, B. D.; Stokes, K. K.; Kumar, S. K. Why is Recycling of Postconsumer Plastics so Challenging? *ACS App. Polym. Mater.* **2021**, *3* (9), 4325-4346. DOI: 10.1021/acsapm.1c00648.

(16) Chu, M. Y.; Tu, W. L.; Yang, S. Q.; Zhang, C. Y.; Li, Q. Y.; Zhang, Q.; Chen, J. X. Sustainable chemical upcycling of waste polyolefins by heterogeneous catalysis. *Susmat* **2022**, *2* (2), 161-185. DOI: 10.1002/sus2.55.

(17) Celik, G.; Kennedy, R. M.; Hackler, R. A.; Ferrandon, M.; Tennakoon, A.; Patnaik, S.; LaPointe, A. M.; Ammal, S. C.; Heyden, A.; Perras, F. A.; et al. Upcycling Single-Use Polyethylene into High-Quality Liquid Products. *ACS Cent. Sci.* **2019**, *5* (11), 1795-1803. DOI: 10.1021/acscentsci.9b00722.

(18) Diaz-Silvarrey, L. S.; Zhang, K.; Phan, A. N. Monomer recovery through advanced pyrolysis of waste high density polyethylene (HDPE). *Green Chem.* **2018**, *20* (8), 1813-1823. DOI: 10.1039/c7gc03662k.

(19) Sodero, S. F.; Berruti, F.; Behie, L. A. Ultrapyrolytic cracking of polyethylene - A high yield recycling method. *Chem. Eng. Sci.* **1996**, *51* (11), 2805-2810. DOI: 10.1016/0009-2509(96)00156-x.

(20) Alston, S. M.; Arnold, J. C. Environmental Impact of Pyrolysis of Mixed WEEE Plastics Part 2: Life Cycle Assessment. *Environ. Sci. Technol.* **2011**, *45* (21), 9386-9392. DOI: 10.1021/es2016654.

(21) Liu, S. B.; Kots, P. A.; Vance, B. C.; Danielson, A.; Vlachos, D. G. Plastic waste to fuels by hydrocracking at mild conditions. *Sci. Adv.* **2021**, *7* (17), eabf8283. DOI: 10.1126/sciadv.abf8283.

(22) Kots, P. A.; Vance, B. C.; Vlachos, D. G. Polyolefin plastic waste hydroconversion to fuels, lubricants, and waxes: a comparative study. *React. Chem. Eng.* **2021**, *7* (1), 41-54. DOI: 10.1039/d1re00447f.

(23) Tennakoon, A.; Wu, X.; Paterson, A. L.; Patnaik, S.; Pei, Y. C.; LaPointe, A. M.; Ammal, S. C.; Hackler, R. A.; Heyden, A.; Slowing, II; et al. Catalytic upcycling of high-density polyethylene via a processive mechanism. *Nat. Catal.* **2020**, *3* (11), 893-901. DOI: 10.1038/s41929-020-00519-4.

(24) Jaydev, S. D.; Martín, A. J.; Usteri, M. E.; Chikri, K.; Eliasson, H.; Erni, R.; Pérez-Ramírez, J. Consumer Grade Polyethylene Recycling via Hydrogenolysis on Ultrafine Supported Ruthenium Nanoparticles. *Angew. Chem., Int. Ed.* **2024**, *63* (11), e202317526. DOI: 10.1002/anie.202317526.

(25) Edenfield, W. C.; Mason, A. H.; Lai, Q. H.; Agarwal, A.; Kobayashi, T.; Kratish, Y.; Marks, T. J. Rapid Polyolefin Plastic Hydrogenolysis Mediated by Single-Site Heterogeneous Electrophilic/Cationic Organo-group IV Catalysts. *ACS Catal.* **2023**, *14* (1), 554-565. DOI: 10.1021/acscatal.3c05161.

(26) Hu, P.; Zhang, C. Y.; Chu, M. Y.; Wang, X. P.; Wang, L.; Li, Y. Y.; Yan, T. R.; Zhang, L.; Ding, Z. F.; Cao, M. H.; et al. Stable Interfacial Ruthenium Species for Highly Efficient Polyolefin Upcycling. *J. Am. Chem. Soc.* **2024**, *146* (10), 7076-7087. DOI: 10.1021/jacs.4c00757.

(27) Rejman, S.; Vollmer, I.; Werny, M. J.; Vogt, E. T. C.; Meirer, F.; Weckhuysen, B. M. Transport limitations in polyolefin cracking at the single catalyst particle level. *Chem. Sci.* **2023**, *14* (37), 10068-10080. DOI: 10.1039/d3sc03229a.

(28) Balzer, A.; Hinton, Z.; Vance, B.; Vlachos, D.; Korley, L.; Epps, T. I. Tracking Chain Populations and Branching Structure during Polyethylene Deconstruction Processes. *ACS Cent. Sci.* **2024**, *10*, 1755-1764. DOI: 10.1021/acscentsci.4c00951.

(29) Kang, Q. Y.; Chu, M. Y.; Xu, P. P.; Wang, X. C.; Wang, S. Q.; Cao, M. H.; Ivasenko, O.; Sham, T. K.; Zhang, Q.; Sun, Q. M.; et al. Entropy Confinement Promotes Hydrogenolysis Activity for Polyethylene Upcycling. *Angew. Chem., Int. Ed.* **2023**, *62* (47), e202313174. DOI: 10.1002/anie.202313174.

(30) O'Shaughnessy, B.; Vavylonis, D. Irreversible adsorption from dilute polymer solutions. *Eur. Phys. J. E* **2003**, *11* (3), 213-230. DOI: 10.1140/epje/i2003-10015-9.

(31) Kumar, S. K.; Jimenez, A. M. Polymer adsorption - reversible or irreversible? *Soft Matter* **2020**, *16* (23), 5346-5347. DOI: 10.1039/d0sm90097d.

(32) Shimokita, K.; Yamamoto, K.; Miyata, N.; Shibata, M.; Nakanishi, Y.; Arakawa, M.; Takenaka, M.; Kida, T.; Tokumitsu, K.; Tanaka, R.; et al. Neutron Reflectivity Study on the Adsorption Layer of Polyethylene Grown on Si Substrate. *Langmuir* **2024**, *40*, 15758-15766. DOI: 10.1021/acs.langmuir.4c01584.

(33) Zare, M.; Kots, P. A.; Hinton, Z. R.; Epps, T. H., III; Korley, L. T. J.; Caratzoulas, S.; Vlachos, D. G. Effect of reaction media on hydrogenolysis of polyethylene plastic waste: Polymer-surface interactions in small alkane/polymer blends. *Appl. Catal., B* **2024**, *351,* 123969. DOI: 10.1016/j.apcatb.2024.123969.

(34) Guisnet, M.; Magnoux, P. Organic chemistry of coke formation. *Appl. Catal., A* **2001**, *212* (1-2), 83-96. DOI: 10.1016/s0926-860x(00)00845-0.

(35) Bhasin, M. M.; McCain, J. H.; Vora, B. V.; Imai, T.; Pujadó, P. R. Dehydrogenation and oxydehydrogenation of paraffins to olefins. *Appl. Catal., A* **2001**, *221* (1-2), 397-419. DOI: 10.1016/s0926-860x(01)00816-x.

(36) Rorrer, J.; Troyano-Valls, C.; Beckham, G.; Román-Leshkov, Y. Hydrogenolysis of Polypropylene and Mixed Polyolefin Plastic Waste over Ru/C to Produce Liquid Alkanes. *ACS Sustainable Chem. Eng.* **2021**, *9*, 11661-11666. DOI: 10.1021/acssuschemeng.1c03786.

(37) Flaherty, D.; Hibbitts, D.; Iglesia, E. Metal-Catalyzed C-C Bond Cleavage in Alkanes: Effects of Methyl Substitution on Transition-State Structures and Stability. *J. Am. Chem. Soc.* **2014**, *136*, 9664-9676. DOI: 10.1021/ja5037429.

(38) Subramanian, P. M. Plastics recycling and waste management in the US. *Resour., Conserv. Recycl.* **2000**, *28* (3-4), 253-263. DOI: 10.1016/s0921-3449(99)00049-x.

(39) Boldizar, A.; Jansson, A.; Gevert, T.; Moller, K. Simulated recycling of post-consumer high density polyethylene material. *Polym. Degrad. Stab.* **2000**, *68* (3), 317-319. DOI: 10.1016/s0141-3910(00)00012-4.

(40) Law, K.; Sobkowicz, M.; Shaver, M.; Hahn, M. Untangling the chemical complexity of plastics to improve life cycle outcomes. *Nat. Rev. Mater.* **2024**, *9*, 657-667. DOI: 10.1038/s41578-024-00705-x.

(41) Sun, J.; Dong, J.; Gao, L.; Zhao, Y.; Moon, H.; Scott, S. Catalytic Upcycling of Polyolefins. *Chem. Rev.* **2024**, *124*, 9457-9579. DOI: 10.1021/acs.chemrev.3c00943.

(42) Jaydev, S. D.; Martin, A. J.; Garcia, D.; Chikri, K.; Perez-Ramirez, J. Assessment of Transport Phenomena in Catalyst Effectiveness for Chemical Polyolefin Recycling. *Nat. Chem.Eng.* **2024**, *1*, 565-575. DOI: 10.1038/s44286-024-00108-3.

(43) Breman, B.; Beenackers, A.; Rietjens, E.; Stege, R. Gas-Liquid Solubilities Of Carbon-Monoxide, Carbon-Dioxide, Hydrogen, Water, 1-Alcohols (1-Less-Than-Or-Equal-To-N-Less-Than-Or-Equal-To-6), And N-Paraffins (2-Less-Than-Or-Equal-To-N-Less-Than-Or-Equal-To-6) In Hexadecane, Octacosane, 1-Hexadecanol, Phenanthrene, And Tetraethylene Glycol At Pressures Up To 5.5 MPA And Temperatures From 293 To 553-K. *J. Chem.Eng. Data* **1994**, *39*, 647-666. DOI: 10.1021/je00016a004.

(44) Hibbitts, D.; Flaherty, D.; Iglesia, E. Effects of Chain Length on the Mechanism and Rates of Metal-Catalyzed Hydrogenolysis of *n*-Alkanes. *J. Phys. Chem. C* **2016**, *120*, 8125-8138. DOI: 10.1021/acs.jpcc.6b00323.

(45) Flaherty, D.; Iglesia, E. Transition-State Enthalpy and Entropy Effects on Reactivity and Selectivity in Hydrogenolysis of *n*-Alkanes. *J. Am. Chem. Soc.* **2013**, *135*, 18586-18599. DOI: 10.1021/ja4093743.

(46) Gin, P.; Jiang, N.; Liang, C.; Taniguchi, T.; Akgun, B.; Satija, S. K.; Endoh, M. K.; Koga, T. Revealed architectures of adsorbed polymer chains at solid-polymer melt interfaces. *Phys. Rev. Lett.* **2012**, *109* (26), 265501. DOI: 10.1103/PhysRevLett.109.265501

(47) Praserthdam, P.; Ayutthaya, S. Roles of NO and O_2 on coke deposition and removal over Cu-ZSM-5. *Catal. Today* **2004**, *97*, 137-143. DOI: 10.1016/j.cattod.2004.04.060.

(48) Choudhary, V.; Sivadinarayana, C.; Devadas, P.; Sansare, S.; Magnoux, P.; Guisnet, M. Characterization of coke on H-gallosilicate (MFI) propane aromatization catalyst. Influence of coking conditions on nature and removal of coke. *Microporous Mesoporous Mater.* **1998**, *21*, 91-101. DOI: 10.1016/S1387-1811(97)00054-1.

(49) Zhang, Y.; Yao, W.; Fang, H.; Hu, A.; Huang, Z. Catalytic alkane dehydrogenations. *Sci. Bull.* **2015**, *60* (15), 1316-1331. DOI: 10.1007/s11434-015-0818-8.

(50) Melnikov, D. P.; Novikov, A. A.; Glotov, A. P.; Reshetina, M. V.; Smirnova, E. M.; Wang, H. Q.; Vinokurov, V. A. Dehydrogenation of Light Alkanes (A Review). *Pet. Chem.* **2022**, *62* (9), 1027-1046. DOI: 10.1134/s096554412209006.

(51) Kim, S.; Sasmaz, E.; Lauterbach, J. Effect of Pt and Gd on coke formation and regeneration during JP-8 cracking over ZSM-5 catalysts. *Appl. Catal., B* **2015**, *168*, 212-219. DOI: 10.1016/j.apcatb.2014.12.027.

(52) Housmans, C.; Sferrazza, M.; Napolitano, S. Kinetics of Irreversible Chain Adsorption. *Macromolecules* **2014**, *47*, 3390-3393. DOI: 10.1021/ma500506r.

(53) Thoms, E.; Song, Z.; Wang, K.; Napolitano, S. Simple Model to Predict the Adsorption Rate of Polymer Melts. *Phys. Rev. Lett.* **2024**, *132,* 248101. DOI: 10.1103/PhysRevLett.132.248101.

(54) Fetters, L.; Lohse, D.; Milner, S.; Graessley, W. Packing length influence in linear polymer melts on the entanglement, critical, and reptation molecular weights. *Macromolecules* **1999**, *32*, 6847-6851. DOI:10.1021/ma990620o

(55) Koga, T.; Jiang, N.; Gin, P.; Endoh, M. K.; Narayanan, S.; Lurio, L. B.; Sinha, S. K. Impact of an irreversibly adsorbed layer on local viscosity of nanoconfined polymer melts. *Phys. Rev. Lett.* **2011**, *107* (22), 225901. DOI: 10.1103/PhysRevLett.107.225901.

(56) Gin, P.; Jiang, N.; Liang, C.; Taniguchi, T.; Akgun, B.; Satija, S. K.; Endoh, M. K.; Koga, T. Revealed Architectures of Adsorbed Polymer Chains at Solid-Polymer Melt Interfaces. *Phys. Rev. Lett.* **2012**, *109* (26), 265501. DOI: 10.1103/PhysRevLett.109.265501.

(57) Napolitano, S.; Capponi, S.; Vanroy, B. Glassy dynamics of soft matter under 1D confinement: How irreversible adsorption affects molecular packing, mobility gradients and orientational polarization in thin films. *Eur. Phys. J. E* **2013**, *36* (61), 61. DOI: 10.1140/epje/i2013-13061-8.

(58) Givens, S.; Gardner, K.; Rabolt, J.; Chase, D. High-temperature electrospinning of polyethylene microfibers from solution. *Macromolecules* **2007**, *40*, 608-610. DOI: 10.1021/ma062398a.

(59) Degennes, P. G. Scaling theory of polymer adsorption. *J. Phys. (Paris)* **1976**, *37* (12), 1445-1452. DOI: 10.1051/jphys:0197600370120144500.

(60) Semenov, A. N.; Avalos, J. B.; Johner, A.; Joanny, J. F. Adsorption of polymer solutions onto a flat surface. *Macromolecules* **1996**, *29* (6), 2179-2196. DOI: 10.1021/ma950712n.

For Table of Contents Only